

Contact dependence of carrier injection in carbon nanotubes: An *ab initio* study

Norbert Nemeč,¹ David Tománek,² and Gianaurelio Cuniberti¹

¹*Institute for Theoretical Physics, University of Regensburg, D-93040 Regensburg, Germany*

²*Physics and Astronomy Department, Michigan State University, East Lansing, Michigan 48824-2320*

(Dated: August 25, 2005)

We combine *ab initio* density functional theory with transport calculations to provide a microscopic basis for distinguishing between ‘good’ and ‘poor’ metal contacts to nanotubes. Comparing Ti and Pd as examples of different contact metals, we trace back the observed superiority of Pd to the nature of the metal-nanotube hybridization. Based on large scale Landauer transport calculations, we suggest that the ‘optimum’ metal-nanotube contact combines a weak hybridization with a large contact length between the metal and the nanotube.

PACS numbers: 73.23.Ad, 73.40.Cg, 73.63.Fg, 73.63.Rt

A major challenge linked to the use of carbon nanotubes [1] in future electronic devices is to understand the profound effect of the nanotube-metal contact on transport. Weak nanotube-metal coupling, found in nanotubes deposited on metal electrodes, has been shown to cause Coulomb blockade behavior [2]. In spite of significant progress in maximizing the contact area by depositing metal on top of nanotubes [3], the transparency of such contacts exhibits strong sample-to-sample variations and depends strongly on the contact metal. Reports of low contact resistance between nanotubes and Au or Au/Cr [4, 5] are in stark contrast to the high resistance observed in nanotube contacts with Au/Ti [6]. The transparency of Pd-based contacts has been reported as superior in comparison to using Ti, Pt and Al as contact metals [7, 8, 9]. Additional modulation of the Pd-nanotube contact transparency has been reportedly achieved by modulating the gate voltage [10]. Reports suggesting that carrier injection occurs only at the edge of the contact region [8] appear to contradict the observed dependence of the contact resistance on the length of the contact [6].

Published theoretical results include studies of the electronic structure at a nanotube-Au interface and transport properties of a nanotube-Al junction [11]. *Ab initio* calculations furthermore suggest that Ti contacts may be superior to those with Al or Au [12], and that the Schottky barrier between semiconducting tubes and Pd is lower than with Au or Pt [13]. Due to the limitation to specific contact geometries and small system dimensions, however, general trends are hard to extract, and an extrapolation to experimentally relevant system sizes is difficult.

Here we combine *ab initio* electronic structure studies with large scale transport calculations to gain microscopic insight into the relative importance of the interface morphology, the type of the contact metal, and the length of the contact region when optimizing the metal-nanotube contact. *Ab initio* density functional studies were used to determine the charge redistribution and electrostatic potential in the contact region. In a second

step, the electronic structure results were mapped onto a model tight-binding Hamiltonian suitable for transport calculations. We found that transmission is maximized in the case of weak metal-nanotube coupling, exhibited by Pd, and extended contacts.

To gain insight into the electronic structure in the contact region, we performed density functional theory (DFT) calculations of Ti and Pd monolayers interacting with a graphene layer. We described valence electrons by Troullier-Martins pseudopotentials and used the Perdew-Zunger form of the exchange-correlation functional in the local density approximation (LDA) to DFT, as implemented in the SIESTA code [14]. With a double-zeta basis and a 100 Ry energy cutoff in the plane-wave expansions of the electron density and potential, we found the total energy to be converged to $\lesssim 1$ meV/atom. We performed a full structure optimization to determine the equilibrium adsorption geometry, the adsorption energy, and the local charge redistribution caused by the metal-graphene interaction. Since the interatomic distances in bulk Pd (2.7 Å) and Ti (2.95 Å) lie close to the honey-

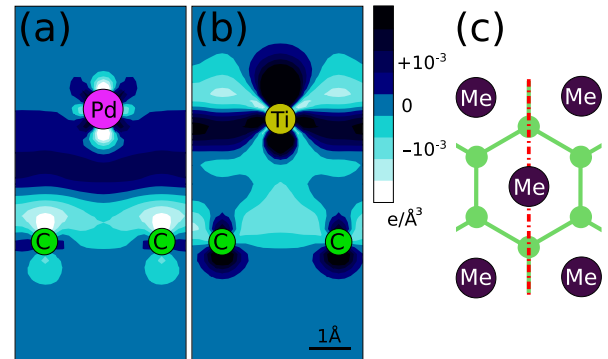


FIG. 1: (Color online) Charge density redistribution $\Delta\rho(r) = \rho_{Me/C}(r) - \rho_{Me}(r) - \rho_C(r)$ in (a) Pd and (b) Ti monolayers interacting with a graphene layer, indicating regions of charge depletion and excess with respect to the superposition of isolated layers. (c) Schematic double-layer geometry in top view, with the cutting plane used in (a) and (b) indicated by the dash-dotted line.

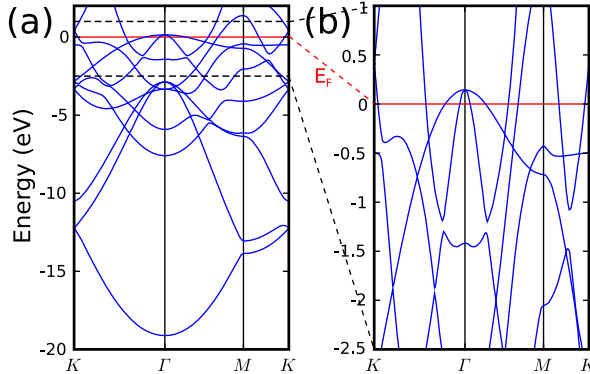


FIG. 2: (Color online) (a) Electronic band structure $E(k)$ of a Pd monolayer interacting with a graphene layer. (b) Details of $E(k)$ in (a) near the Fermi level, defined as $E_F = 0$.

comb spacing in graphene (2.46 Å), we only considered epitaxial adsorption. For both Pd and Ti, we found a slight preference for the sixfold hollow site on graphite, depicted schematically in Fig. 1(c). For Pd, we found the equilibrium inter-layer distance to be 3.2 Å, consistent with a relatively weak, mostly covalent bond energy of 0.3 eV per Pd atom. The interaction between an epitaxial Ti monolayer and graphene was only insignificantly stronger with 0.4 eV per Ti atom at an inter-layer distance of 3.0 Å.

The quality of nanotube-electrode contacts has been shown to depend sensitively on the Schottky-barrier in semiconducting nanotubes [15] and band bending in metallic nanotubes, both reflecting the charge transfer within the junction. Our Mulliken population analysis indicates a net charge transfer of only ≈ 0.1 electrons from Pd and Ti to the graphene layer. More useful information is contained in the charge redistribution, depicted in Fig. 1. Results for Pd electrodes, shown in Fig. 1(a), suggest an accumulation of excess charge in the region between Pd and graphene layers. As seen in Fig. 1(b), the charge redistribution in Ti/graphene is very different, suggesting charge accumulation in the atomic layers and depopulation of the interlayer region and thus an increase of the interlayer scattering potential. The lower scattering potential and the populated interlayer state at the Pd/C junction appear well suited for carrier injection into the nanotube, making the Pd/C contact superior to the Ti/C contact.

Besides the charge transfer, the contact quality depends even more sensitively on the nanotube-metal hybridization [16], which is addressed in Fig. 2 for the Pd/graphene system. The density of states (DOS) at E_F assumes a large value, which is a pre-requisite for a good contact. The electronic band structure of the system, depicted in Fig. 2(a), suggests that all states are closely related to either Pd or graphene states. In the Pd/graphene system, the graphene bands are rigidly shifted by $\Delta E_C = 0.374$ eV and the metal bands by

$\Delta E_{\text{Pd}} = -0.020$ eV with respect to the isolated layers. In the Ti/graphene system, the rigid band shift at the junction is much stronger, $\Delta E_C = -1.15$ eV, and has the opposite sign to Pd.

Especially interesting for the transparency of the contact is the nature of Pd-C rehybridization, which is best visible in Fig. 2(b) close to the Fermi level. Particularly clear is the hybridization between $\text{Pd}d_{z^2}$ and $\text{C}p_z$ orbitals, which causes a ≈ 0.15 eV band splitting about 0.5 eV below E_F , in the vicinity of the K point. Since K denotes also the Fermi momentum of graphene, this occurrence of Pd-C hybridization near this k -point suggests an efficient way to inject carriers into graphene near the Fermi energy without involving phonons to conserve momentum.

To obtain quantitative information about the effect of the junction geometry and hybridization on the transparency of the contact, we performed large scale quantum transport calculations of nanotubes in contact with metal electrodes within the Landauer approach [17]. Our calculations for nanotube segments exceeding 10^2 nm were facilitated using an efficient $O(N)$ decimation algorithm [18]. Our transport calculations were based on a simplified tight-binding Hamiltonian, describing only the interaction between $\text{Pd}d_{z^2}$ and $\text{C}p_z$ orbitals. We found that the electronic band structure of the Pd/graphene system near E_F , depicted in Fig. 2(b), can be reproduced by considering the hybridization between the $pp\pi$ band of graphene, associated with $\gamma_0 = 2.66$ eV, and a Pd-based band, using $t_{\text{Pd/C}} \approx 0.15$ eV for the hopping integral between Pd and each of the six C neighbors. Such a simple mapping turned out insufficient to describe the hybridization between Ti and graphene. Based on typical band repulsion observed in that system, the Ti-C hopping integral $t_{\text{Ti/C}} \approx 0.3$ eV should be about twice that found for Pd.

Results of our transport calculations for metal-nanotube junctions are summarized in Fig. 3. In our schematic view of an extended contact, depicted in Fig. 3(a), we distinguish three regions within a finite tube. The central region of length L_0 , describing an unperturbed nanotube, is connected at both ends to contact regions of varying length L_c . In both extended contact regions, each atom is coupled to the coating metal electrode in a similar way, as previously considered in Ref. [19].

In the model examined in the following, we chose diagonal wide-band leads, which contacted each atom of the nanotube independently. In this case, the coupling is described by an energy-independent, purely imaginary self energy $\Sigma(E) = -i\Delta$, where $\Delta = t_{\text{Me/C}}^2 \mathcal{N}_{\text{Me}}(E_F)$ can be extracted from our *ab initio* results. Using the calculated density of states $\mathcal{N}_{\text{Me}}(E_F)$ at Pd and Ti surfaces, which is of the order 1 eV^{-1} , we obtain $\Delta_{\text{Pd}} \approx 0.06$ eV and $\Delta_{\text{Ti}} \approx 0.3$ eV, assuming that each carbon atom is in direct contact with three metal atoms.

Transmission T through a molecular conductor is gen-

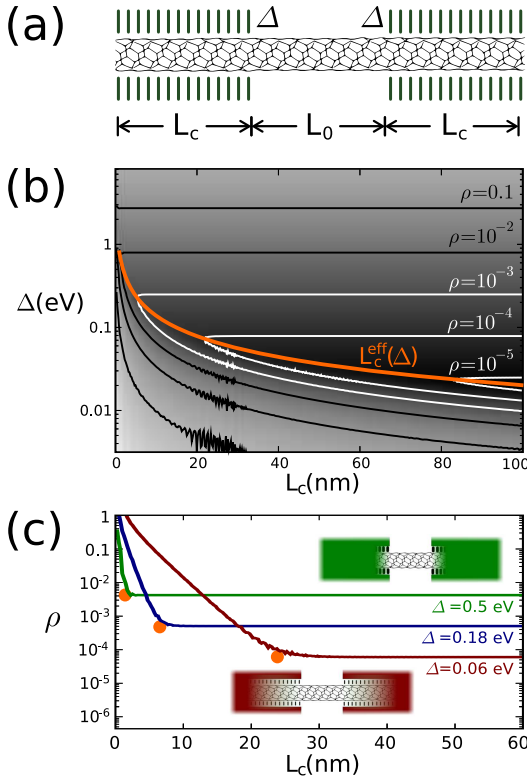


FIG. 3: (Color online) (a) Schematic geometry of the (6,6) nanotube in contact with metal leads, used in the calculation of the contact reflection coefficient ρ . (b) Contact reflection coefficient ρ as a function of the nanotube-metal coupling Δ and the contact length L_c . (c) Cuts through the contour plot (b) at selected values of Δ , showing ρ as a function of L_c . The effective contact length L_c^{eff} is emphasized by a heavy solid line in (b) and by data points in (c).

erally limited by the number of channels N_{ch} , which depends on the band structure of a perfectly periodic system as $T \leq T_{\text{bands}} = N_{\text{ch}}$. The reason for the effective transmission through a conductor with contacts $T(L_c, \Delta)$ being lower than through the ideal infinite system T_{bands} lies in the reflection at the contacts. To quantify the quality of a nanotube contact, we define the contact reflection coefficient by

$$\rho(L_c, \Delta) = \frac{1}{\langle T(L_c, \Delta) \rangle} - \frac{1}{T_{\text{band}}} . \quad (1)$$

The average is taken around the Fermi level, in a region between the first van-Hove singularities, similar to a transmission convolution capturing hot electron effects [20]. Our results in Fig. 3, based on ensemble averaging in Eq. (1), agree quantitatively with those obtained by averaging the transmission using the Fermi distribution, for a wide range of temperatures. Physically, the total resistance R of such an idealized system could be separated as $R = R_{\text{band}} + R_c$, where $R_{\text{band}} = 1/(2G_0)$ is given by the quantum limit of two open channels with conductance $G_0 = 2e^2/h$ each. Assuming zero temper-

ature and neglecting disorder effects, $R_c \sim \rho/G_0$ originates only from sub-optimal contacts and may theoretically be arbitrarily small.

We generally expect zero transmission in the limiting cases of vanishing contact length, $L_c = 0$, and vanishing coupling, $\Delta = 0$. For finite values of L_c and Δ , however, it is not obvious if a combination of strong coupling and short contact is superior to a combination of weak coupling and a long contact. To obtain a quantitative answer, we calculated ρ for a contact to a (6,6) armchair nanotube with $L_0 = 100$ nm as a function of L_c and Δ . We found ρ to be independent of the tube diameter, as long as the energy range used in the averaging avoids subband-related van Hove singularities. We also found no dependence on L_0 , as long as L_0 was much larger than a unit cell size. Consequently, ρ should be only a function of L_c and Δ .

Our results for $\rho(L_c, \Delta)$ are depicted in Figs. 3(b) and (c). We find the contour plot of ρ in Fig. 3(b) separated into two regions by a line of “minimum contact reflection” $L_c^{\text{eff}}(\Delta)$. In short contacts, the transparency is restricted by L_c and ρ increases with decreasing L_c due to a generalized Breit-Wigner broadening of the resonances. The pronounced ripples found at small values of Δ and L_c are not numerical artefacts, but rather reflect the interplay between resonances in a finite nanotube segment and conduction electrons propagating with the Fermi momentum. For very weak coupling, we find $\langle T \rangle_E \propto L_c \Delta$. For larger values of $L_c \Delta$, however, dissipation along the contact region modifies this simple behavior, yielding $\rho \propto \exp(-\alpha L_c \Delta)$.

In sufficiently long contacts, defined by $L_c > L_c^{\text{eff}}$, ρ becomes independent of L_c and is given by $\rho = \rho_0 \Delta^2$. We found that our results can be reproduced well by using $\rho_0 = 0.016 \text{ eV}^{-2}$. The independence of ρ from L_c in long contacts is seen clearly in the plots of $\rho(L_c)$, depicted in Fig. 3(c) for selected values of Δ . Particularly intriguing appears our result that reflection is minimized in case of a weaker specific coupling, provided the contact is sufficiently long.

This physical origin of this unexpected behavior is schematically illustrated in the insets in Fig. 3(c). Saturation transparency is reached for relatively short contacts in the case of strong coupling. In this case, however, the abrupt change in the electronic structure between the uncoated and the coated nanotube segment causes extra reflection. This change is less abrupt in the case of weaker coupling and a long effective contact region L_c^{eff} , reducing the overall reflection.

To estimate the effective contact length L_c^{eff} , we make use of the above described expressions for ρ in the adjacent regions in the (L_c, Δ) plane. The line, where these two functions intersect, corresponds to the line of minimum ρ , and is given by the analytical expression

$$L_c^{\text{eff}}(\Delta) = \ell_{\text{uc}} \frac{\alpha_1}{\Delta} \ln \frac{\alpha_2}{\Delta} . \quad (2)$$

Here, $\ell_{uc} = 2.46 \text{ \AA}$ is the unit cell length. The parameters $\alpha_1 = 1.34 \text{ eV}$ and $\alpha_2 = 9.14 \text{ eV}$ were obtained by fitting our numerical data. In the specific case of Pd and Ti, we found $L_c^{\text{eff}}(\Delta_{\text{Pd/C}}) \approx 30 \text{ nm}$ and $L_c^{\text{eff}}(\Delta_{\text{Ti/C}}) \approx 4 \text{ nm}$.

Since realistic metal-nanotube contacts are rarely epitaxial, we have considered various forms of disorder in the contact region and determined their effect on transport. We modelled weak to moderate disorder by randomly perturbing the metal-nanotube coupling Δ with respect to $\Delta_{\text{Me/C}}$. We did not find noticeable change in ρ even for perturbations of Δ as large as its reference value. As another extreme case, we modelled strongly diluted contacts by randomly suppressing the interaction between individual metal and nanotube atoms in the contact region, down to one percent of contacts with respect to the epitaxial case. Finally, we considered various forms of non-diagonal contributions to the self-energy, modelling the cross-coupling between neighboring metal atoms. In all the studies, which addressed deviations from epitaxy at the interface and our description of the leads, we found the same behavior as depicted in Fig. 3 and analytically described by Eq. (2), with possibly modified numerical values of ρ_0 , α_1 and α_2 [18].

Our main conclusion, which proved to be robust with respect to variations in the details, is that each contact can be characterized by an effective contact length L_c^{eff} , which depends only on the local metal-nanotube coupling, not on the diameter of the tube. Assuming that the effective contact length between the nanotube and the electrode exceeds L_c^{eff} , which is likely the case in most experimental setups, then a higher contact transparency is expected when the metal-nanotube coupling is weak [19]. Especially in very long contacts, the sensitive $\rho = \rho_0 \Delta^2 \propto t_{\text{Me/C}}^4$ dependence of ρ on the coupling strength $t_{\text{Me/C}}$ may be taken as an important guideline, suggesting to minimize coupling and maximize contact length to achieve a high contact transparency. In the specific case of Pd and Ti contacts, the weaker nanotube-metal coupling in the case of Pd is a good explanation for the superiority of Pd-based nanotube contacts.

In conclusion, we combined *ab initio* density functional theory with transport calculations to distinguish microscopically between ‘good’ and ‘poor’ metal contacts to nanotubes. Comparing Pd and Ti as examples of different contact metals, we traced back the observed superiority of Pd to the nature of the metal-nanotube hybridization. Based on large scale Landauer transport calculations, we suggest that the ‘optimum’ metal-nanotube contact generally combines a weak hybridization with a large contact length of typically few hundred nanometers between the metal and the nanotube.

Of immediate interest is, of course, the general validity of our results. We plan additional studies addressing the effect of non-epitaxial contacts and the nature of charge carriers [18]. Particularly interesting in this respect should be studying spin injection from ferromag-

netic contacts and Andreev reflection at the contact to superconducting electrodes.

We acknowledge fruitful discussions with M. Grifoni, A. Nitzan, J. Fabian and C. Strunk. This work has been funded by the Volkswagen Stiftung under grant No. I/78 340. DT was partially supported by the Vielberth Foundation, the DFG-GRK 638, NSF-NIRT grants DMR-0103587, ECS-0506309, and NSF NSEC Grant No. 425826.

- [1] S. Iijima, *Nature* **354**, 56 (1991).
- [2] S. J. Tans, M. H. Devoret, H. Dai, A. Thess, R. E. Smalley, L. J. Geerligs, and C. Dekker, *Nature* **386**, 474 (1997).
- [3] M. Bockrath, W. Liang, D. Bozovic, J. H. Hafner, C. M. Lieber, M. Tinkham, and H. Park, *Science* **291**, 283 (2001).
- [4] Y. Yaish, J.-Y. Park, S. Rosenblatt, V. Sazonova, M. Brink, and P. L. McEuen, *Phys. Rev. Lett.* **92**, 046401 (2004).
- [5] W. Liang, M. Bockrath, D. Bozovic, J. H. Hafner, M. Tinkham, and H. Park, *Nature* **411**, 665 (2001).
- [6] F. Wakaya, K. Katayama, and K. Gamo, *Microelectronic Engineering* **67-68**, 853 (2003).
- [7] A. Javey, J. Guo, Q. Wang, M. Lundstrom, and H. Dai, *Nature* **424**, 654 (2003).
- [8] D. Mann, A. Javey, J. Kong, Q. Wang, and H. Dai, *Nano Lett.* **3**, 1541 (2003).
- [9] Z. Chen, J. Appenzeller, J. Knoch, Y.-M. Lin, and P. Avouris, *Nano Lett.* **5**, 1497 (2005).
- [10] B. Babić and C. Schönenberger, *Phys. Rev. B* **70**, 195408 (2004).
- [11] Marco Buongiorno Nardelli, J.-L. Fattebert, and J. Bernholc, *Phys. Rev. B* **64**, 245423 (2001); Angel Rubio, Daniel Sánchez-Portal, Emilio Artacho, Pablo Ordejón, and José M. Soler, *Phys. Rev. Lett.* **82**, 3520 (1999).
- [12] J. J. Palacios, A. J. Pérez-Jiménez, E. Louis, E. San-Fabián, and J. A. Vergés, *Phys. Rev. Lett.* **90**, 106801 (2003).
- [13] B. Shan and K. Cho, *Phys. Rev. B* **70**, 233405 (2004).
- [14] J. M. Soler, E. Artacho, J. D. Gale, A. García, J. Junquera, P. Ordejón, and D. Sánchez-Portal, *J. Phys: Condens. Matter* **14**, 2745 (2002).
- [15] S. Heinze, J. Tersoff, R. Martel, V. Derycke, J. Appenzeller, and P. Avouris, *Phys. Rev. Lett.* **89**, 106801 (2002).
- [16] J. Knoch, S. Mantl, Y. Min, Z. Chen, P. Avouris, and J. Appenzeller, in *Device Research Conference* (2004), pp. 135–136.
- [17] G. Cuniberti, F. Großmann, and R. Gutiérrez, *Advances in Solid State Physics* **42**, 133 (2002).
- [18] N. Nemec, D. Tománek, and G. Cuniberti, unpublished.
- [19] T. Nakanishi and T. Ando, *J. Phys. Soc. Japan* **69**, 2175 (2000).
- [20] An alternative definition $\rho = \langle 1/T \rangle - 1/T_{\text{band}}$ would differ from Eq. (1) only in the high- ρ regime, which is not of primary interest here.